THE JOURNAL OF PHYSICAL CHEMISTRY Letters

Letter

pubs.acs.org/JPCL

Ab Initio Nonadiabatic Dynamics with Coupled Trajectories: A Rigorous Approach to Quantum (De)Coherence

Seung Kyu Min,*[,†] Federica Agostini,*[,‡] Ivano Tavernelli,[¶] and E. K. U. Gross[§]

[†]Department of Chemistry, School of Natural Science, Ulsan National Institute of Science and Technology (UNIST), Ulsan 44919, Korea

[‡]Laboratoire de Chimie Physique, UMR 8000 CNRS/University Paris-Sud, University Paris-Saclay, 91405 Orsay, France

[¶]IBM Research GmbH, Zürich Research Laboratory, 8803 Rüschlikon, Switzerland

[§]Max-Planck Institut für Mikrostrukturphysik, Weinberg 2, D-06120 Halle, Germany

Supporting Information

ABSTRACT: We report the first nonadiabatic molecular dynamics study based on the exact factorization of the electron−nuclear wave function. Our approach (a coupled-trajectory mixed quantum−classical, CT-MQC, scheme) is based on the quantum−classical limit derived from systematic and controlled approximations to the full quantum-mechanical problem formulated in the exact-factorization framework. Its strength is the ability to correctly capture quantum (de)coherence effects in a trajectory-based approach to excited-state dynamics. We show this by benchmarking CT-MQC dynamics against a revised version of the popular fewest-switches surface-hopping scheme that is able to fix its well-documented overcoherence issue. The CT-MQC approach is successfully applied to investigation of the photochemistry (ring-opening) of oxirane in the gas phase, analyzing in detail the role of decoherence. This work represents a significant step forward in the establishment of the exact factorization as a powerful tool to study excited-state dynamics, not only for interpretation purposes but mainly for nonadiabatic ab initio molecular dynamics simulations.

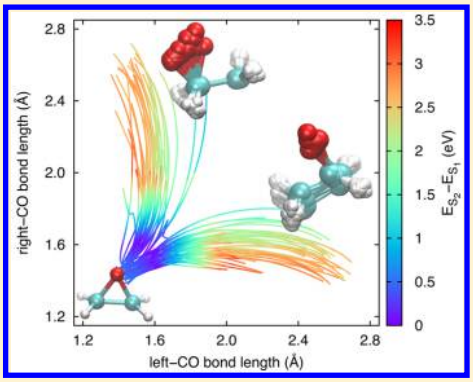

Quantum coherence in excited-state dynamics is a challenging problem that has attracted increasing interest in the Physical Chemistry community.[1−13] In the conventional picture derived within the Born−Oppenheimer framework, the time evolution of the molecular wave function is separated into electronic and nuclear subsystem dynamics, which however remain entangled through the nonadiabatic coupling. It is this coupling that induces decoherence effects, leading, far from any coupling region, to the "collapse" of the electronic subsystem onto a selected final (adiabatic) state. From a theoretical perspective, decoherence is defined via the reduced density matrix, whose off-diagonal elements describe the coherences. (Within this definition, quantum (de)-coherence becomes clearly a representation-dependent quantity.) As a genuine quantum phenomenon, (de)coherence is difficult to capture using approximate numerical solutions of the time-dependent Schrödinger equation for the combined electron−nuclear wave function. This is especially true when a mixed quantum−classical approximation to the coupled dynamics is employed, where an ensemble of trajectories is introduced to mimic the nuclear wavepacket evolution. While transition probabilities and branching ratios are often well described in this way, the classical description of the nuclear degrees of freedom hampers an adequate description of quantum coherence and decoherence effects. Alternative approaches[14−22] based on nuclear wavepacket dynamics can better capture quantum effects, but their applicability is limited by the number of accessible degrees of freedom.

Due to the complexity of the coupled electron−nuclear dynamics, the simulation of photophysics and photochemistry of molecular systems in their full (unconstrained) configuration space requires the use of mixed quantum−classical molecular dynamics approaches. Therefore, the development of reliable approaches describing quantum mechanical coherence and decoherence effects using trajectory-based approaches is of paramount importance. Such approaches will offer a solid basis for the interpretation of experimentally observed quantum (de)coherence phenomena, reducing the level of uncertainty resulting from the available approximations.[7,23−26]

Over the years, a plethora of trajectory-based approaches to excited-state dynamics have been proposed, aiming to correctly capture quantum decoherence. Among the most prominent examples are the quantum−classical Liouville equation,[27−32] the (linearized) path-integral representation of correlation functions,[33−35] nonadiabatic Bohmian dynamics,[36,37] the conditional wave function approach,[38] as well as different revised versions of the Ehrenfest method[39−42] and of the surface-

Received: May 18, 2017
Accepted: June 16, 2017
Published: June 16, 2017

DOI: 10.1021/acs.jpclett.7b01249
J. Phys. Chem. Lett. 2017, 8, 3048−3055

hopping scheme.[43−48] The latter are probably the most popular approaches as they can be easily implemented and combined with on-the-fly ab initio electronic structure calculations.[49−52] Ehrenfest dynamics, in its original mean-field formulation, may generate unphysical nuclear dynamics due to the impossibility to capture branching along different paths in configuration space. The stochastic nature of the surface-hopping algorithm,[53,54] instead, allows one to overcome this problem but still induces overcoherence effects based on an independent-trajectory approximation.[55] As a consequence, a large amount of literature has been devoted to deal with the overcoherence problem of surface hopping in different ways.[44,56−62]

Starting from the exact factorization of the electron−nuclear wave function,[63,64] an alternative trajectory-based algorithm to excited-state dynamics was recently proposed.[65−67] The coupled-trajectory mixed quantum−classical (CT-MQC) algorithm developed from the exact decomposition of the electron−nuclear dynamics allows one to naturally achieve (i) full control of the approximations introduced to simplify the original equations[65−69] and (ii) the ability of capturing, without the use of empirical a posteriori corrections, subtle quantum-mechanical features as the above-mentioned branching of paths[70] and, above all, quantum decoherence. However, the power of such an algorithm has been shown so far only for a set of model studies.[71,72] It remained an open question[73−75] whether the complexity of the procedure would allow for applications to realistic problems.

In this Letter, the exact factorization is employed for the first time for the simulation of photoexcited dynamics in molecules in their full configuration space. Describing the photochemistry of oxirane, we illustrate the performance of the CT-MQC algorithm combined with on-the-fly electronic structure calculations based on time-dependent density functional theory (TDDFT).[76−78] This Letter should not solely be intended as the first molecular application of the CT-MQC scheme but also as the completion of the establishment of the exact factorization in the field of Physical Chemistry as a powerful tool for the understanding of excited-state dynamics.

In the exact factorization,[63,64] the solution of the time-dependent Schrödinger equation $\hat{H}(\boldsymbol{r},\boldsymbol{R})\Psi(\boldsymbol{r},\boldsymbol{R},t) = i\hbar\partial_t\Psi(\boldsymbol{r},\boldsymbol{R},t)$ is written as a single product $\Psi(\boldsymbol{r},\boldsymbol{R},t) = \chi(\boldsymbol{R},t)\Phi_{\boldsymbol{R}}(\boldsymbol{r},t)$ of a nuclear wave function and an electronic factor that parametrically depends on the nuclear configuration. The whole set of electronic and nuclear coordinates is indicated as $\boldsymbol{r}$ and $\boldsymbol{R}$, respectively, and the molecular Hamiltonian $\hat{H}(\boldsymbol{r},\boldsymbol{R}) = \hat{T}_n(\boldsymbol{R}) + \hat{H}_{BO}(\boldsymbol{r},\boldsymbol{R})$ comprises the nuclear kinetic energy, $\hat{T}_n(\boldsymbol{R})$, and the electronic Born−Oppenheimer (BO) Hamiltonian, $\hat{H}_{BO}(\boldsymbol{r},\boldsymbol{R})$, containing the electronic kinetic energy and all of the interactions. As a result of the exact factorization, the time-dependent Schrödinger equation is decomposed as coupled evolution equations for the two components of the molecular wave function, namely, $[\hat{H}_{BO}(\boldsymbol{r},\boldsymbol{R}) + \hat{U}_{en}^{coup}[\Phi_{\boldsymbol{R}}\chi] - \epsilon(\boldsymbol{R},t)]\Phi_{\boldsymbol{R}}(\boldsymbol{r},t) = i\hbar\partial_t\Phi_{\boldsymbol{R}}(\boldsymbol{r},t)$ and $[\sum_{\nu=1}^{N_n}\{-i\hbar\nabla_\nu + \boldsymbol{A}_\nu(\boldsymbol{R},t)\}^2/2M_\nu + \epsilon(\boldsymbol{R},t)]\chi(\boldsymbol{R},t) = i\hbar\partial_t\chi(\boldsymbol{R},t)$. The nuclear equation is a standard time-dependent Schrödinger equation with time-dependent vector potential $\boldsymbol{A}_\nu(\boldsymbol{R},t) = \langle\Phi_{\boldsymbol{R}}(t)|-i\hbar\nabla_\nu\Phi_{\boldsymbol{R}}(t)\rangle_r$ and time-dependent scalar potential $\epsilon(\boldsymbol{R},t) = \langle\Phi_{\boldsymbol{R}}(t)|\hat{H}_{BO} + \hat{U}_{en}^{coup} - i\hbar\partial_t|\Phi_{\boldsymbol{R}}(t)\rangle_r$ (also referred to as the time-dependent potential energy surface) accounting for nonadiabatic effects. The symbol $\langle\dots\rangle_r$ denotes integration over the electronic coordinates. The electronic equation describes how the electronic wave function follows nuclear evolution, containing the full dynamical coupling to the nuclear degrees of freedom via the electron−nuclear coupling operator $\hat{U}_{en}^{coup}[\Phi_{\boldsymbol{R}}\chi] = \sum_\nu[(-i\hbar\nabla_\nu - \boldsymbol{A}_\nu)^2/2M_\nu + (-i\hbar\nabla_\nu\chi/\chi + \boldsymbol{A}_\nu)(-i\hbar\nabla_\nu + \boldsymbol{A}_\nu)/M_\nu]$.[64,67,79−82]

A trajectory-based solution of the above electronic and nuclear equations is constructed by (i) determining the classical limit of the nuclear equation, thus deriving the corresponding Newton equation with forces computed from the time-dependent vector $\boldsymbol{A}_\nu(\boldsymbol{R},t)$ and scalar $\epsilon(\boldsymbol{R},t)$ potentials, (ii) introducing the Born−Huang-like expansion of the electronic wave function $\Phi_{\boldsymbol{R}}(\boldsymbol{r},t) = \sum_l C_l(\boldsymbol{R},t)\varphi_{\boldsymbol{R}}^l(\boldsymbol{r})$ in the adiabatic basis (where $\varphi_{\boldsymbol{R}}^l(\boldsymbol{r})$ are the eigenfunctions of $\hat{H}_{BO}$), and (iii) approximating the explicit dependence on the nuclear wave function, that is, the term $-i\hbar\nabla_\nu\chi(\boldsymbol{R})/\chi(\boldsymbol{R})$ above, of the coupling operator $\hat{U}_{en}^{coup}[\Phi_{\boldsymbol{R}}\chi]$ employing information obtained from the trajectories. A thorough account of the steps adopted for the derivation of the algorithm is given in ref 72, and a summary is provided in the Supporting Information. Following this procedure, the electronic and nuclear equations of the exact factorization can be rewritten as

$$\dot{C}_l^{(I)}(t) = \dot{C}_{\mathrm{Eh}.l}^{(I)}(t) + \dot{C}_{\mathrm{qm}l}^{(I)}(t) \qquad \text{and}$$
$$\mathbf{F}_\nu^{(I)}(t) = \mathbf{F}_{\mathrm{Eh}.\nu}^{(I)}(t) + \mathbf{F}_{\mathrm{qm}\nu}^{(I)}(t) \tag{1}$$

The electronic equation yields a set of ordinary differential equations $\dot{C}_l^{(I)}(t)$ for the expansion coefficients in the Born−Huang expansion, each labeled by a superscript (I) indicating that they are calculated along the Ith classical trajectory. The nuclear equation allows one to identify the classical force $\mathbf{F}_\nu^{(I)}(t)$ acting on the νth nucleus that evolves along the Ith trajectory. Both equations can be decomposed as the sum of two terms: the first, indicated by "Eh.", comprises Ehrenfest-like terms, while the second, "qm", originates from the exact factorization. These last terms depend on the so-called "quantum momentum", as described below. The Ehrenfest-like terms are

$$\dot{C}_{\mathrm{Eh}.l}^{(I)}(t) = \frac{-i}{\hbar}\epsilon_{BO}^{(I)(I)}C_l^{(I)}(t) - \sum_k C_k^{(I)}(t)\sum_{\nu=1}^{N_n}\frac{\mathbf{P}_\nu^{(I)}(t)}{M_\nu}\cdot\mathbf{d}_{\nu,lk}^{(I)} \tag{2}$$

$$\mathbf{F}_{\mathrm{Eh}.\nu}^{(I)}(t) = -\sum_k |C_k^{(I)}(t)|^2\nabla_\nu\epsilon_{BO}^{(k),(I)} - \sum_{k,l} C_l^{(I)*}(t)C_k^{(I)}(t)(\epsilon_{BO}^{(k),(I)} - \epsilon_{BO}^{(l),(I)})\mathbf{d}_{\nu,lk}^{(I)} \tag{3}$$

where we introduced the symbols $\epsilon_{BO}^{(l),(I)}$ for the electronic adiabatic potential energy surface corresponding to state l and evaluated at the position of the Ith trajectory, $\mathbf{d}_{\nu,lk}^{(I)}$ for the nonadiabatic coupling vectors defined as $\langle\varphi^{(l)}{}^{(I)}|\nabla_\nu\varphi^{(k),(I)}\rangle_r$ as well evaluated at the position of the trajectory I, and $\mathbf{P}_\nu^{(I)}(t)$ for the classical momentum of the νth nucleus evolving along the Ith trajectory. The additional terms in eq 1, namely

$$\dot{C}_{\mathrm{qm}l}^{(I)}(t) = -\sum_{\nu=1}^{N_n}\frac{Q_\nu^{(I)}(t)}{\hbar M_\nu}\cdot[\sum_k |C_k^{(I)}(t)|^2\mathbf{f}_{k,\nu}^{(I)}(t) - \mathbf{f}_{l,\nu}^{(I)}(t)]C_l^{(I)}(t) \tag{4}$$

$$\mathbf{F}_{\mathrm{qm}\nu}^{(I)}(t) = -\sum_l |C_l^{(I)}(t)|^2\left(\sum_{\nu'=1}^{N_n}\frac{2}{\hbar M_{\nu'}}Q_{\nu'}^{(I)}(t)\cdot\mathbf{f}_{l,\nu'}^{(I)}(t)\right) \times [\sum_k |C_k^{(I)}(t)|^2\mathbf{f}_{k,\nu}^{(I)}(t) - \mathbf{f}_{l,\nu}^{(I)}(t)] \tag{5}$$

can be derived *only* in the context of the exact factorization as they both depend on the quantum momentum[83]

DOI: 10.1021/acs.jpclett.7b01249
J. Phys. Chem. Lett. 2017, 8, 3048−3055

$Q_\nu^{(I)}(t) = -\hbar(\nabla_\nu|\chi^{(I)}(t)|^2)/(2|\chi^{(I)}(t)|^2)$. Here, $|\chi^{(I)}(t)|^2$ stands for the value of the nuclear density evaluated at the position of the Ith trajectory and is computed as described in the Supporting Information. The quantum momentum appears in the expression of $\hat{U}_{\text{en}}^{\text{coup}}[\Phi_R\chi]$ as a purely imaginary correction to the (real-valued) classical momentum. As exhaustively described in ref 72, the evaluation of the quantum momentum along the Ith trajectory at a given time requires knowledge of the positions of all other trajectories at the same time. This peculiar feature couples the trajectories in a nontrivial manner, thus allowing for the correct description of quantum decoherence effects. The additional new quantities appearing in eqs 4 and 5 are the adiabatic forces accumulated over time $\mathbf{f}_{l,\nu}^{(I)}(t) = -\int^t \mathrm{d}t'\, \nabla_\nu \epsilon_{\text{BO}}^{(l),(I)}$.

The implementation of the CT-MQC equations simply requires the calculation of electronic adiabatic energies, adiabatic forces, and nonadiabatic coupling vectors, quantities that are provided by standard electronic structure packages. In fact, eqs 2−5 can be easily included based on the implementation of the surface-hopping algorithm by modifying the calculation of the classical forces and by adapting the electronic evolution equation by adding the $\dot{C}_{\text{qm}\,l}^{(I)}(t)$ term. For this first study, eqs 1−5 have been implemented in CPMD,[84] a plane-wave electronic structure software based on DFT. Excited-state properties are determined in the framework of linear-response TDDFT,[85−87] based on the existing implementation of the surface-hopping scheme of refs 50 and 88.

As an application of the CT-MQC approach, we investigate the photoinduced ring-opening process in oxirane[89,90] triggered by the excitation from S_0 to S_2. Our focus is on presenting the performance of CT-MQC in comparison to fewest-switches[54] surface hopping (FSSH) and to a corrected version of this algorithm[44] (corr-FSSH) that accounts for quantum decoherence in a phenomenological manner. All calculations are performed with the CPMD code using the GGA functional PBE,[91] which allows for consistent analysis and comparison of the results obtained from the different approaches. A detailed discussion on the accuracy of the TDDFT approach and on the effect of the combined use of pseudopotentials and the plane-wave basis set has been reported in ref 90 and will not be repeated here. Further computational details can be found at the end of the Letter.

Figure 1 (upper panel) shows the populations of the electronic states, that is, S_0, S_1, and S_2, as functions of time. CT-MQC dynamics perfectly captures the passage of the trajectories through the S_1/S_2 conical intersection after about 10 fs from the initial excitation, in agreement with FSSH results. The $S_2 \rightarrow S_1$ population transfer is slightly overestimated by FSSH but is corrected by corr-FSSH, with CT-MQC results following the tendency of the correction. In the CT-MQC algorithm, the population of the lth electronic adiabatic state along the dynamics is computed directly from the coefficients of the Born−Huang expansion of the electronic wave function, averaged over the N_{tr} trajectories, that is, $\rho_l(t) = N_{\text{tr}}^{-1}\sum_{I=1}^{N_{\text{tr}}}|C_l^{(I)}(t)|^2$. In the surface-hopping scheme, instead, this quantity is estimated as the ratio between the number of trajectories "running on" surface l at a given time, $N_{\text{tr}}^l(t)$, and the total number of trajectories, that is, $\rho_l^{\text{SH}}(t) = N_{\text{tr}}^l(t)/N_{\text{tr}}$. In the standard surface-hopping procedure, if decoherence effects are important, $\rho_l^{\text{SH}}(t)$ yields electronic populations that differ from those evaluated via an average over trajectories equivalent to $\rho_l(t)$. The decoherence corrections employed here[44] are designed to restore the consistency between the two procedures for estimating electronic populations. When adopting the CT-MQC scheme for the dynamics, such inconsistency is naturally removed as the populations are directly estimated as the average of $|C_l^{(I)}(t)|^2$.

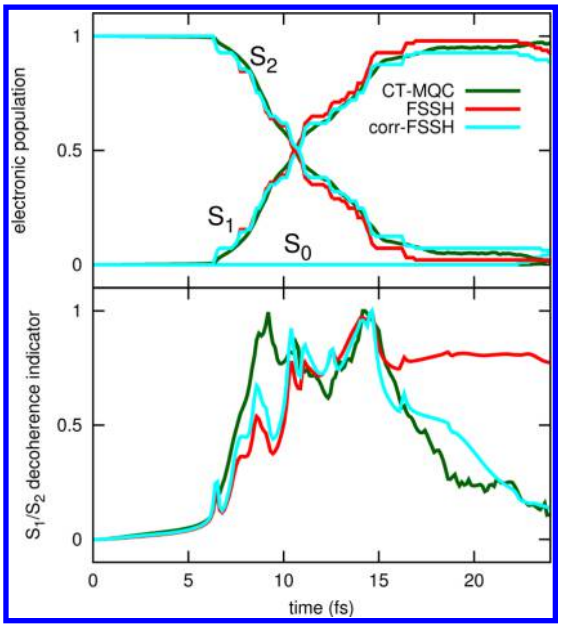

Figure 1. Upper panel: Electronic populations of S_0, S_1, and S_2 as functions of time. Lower panel: Indicator of decoherence for the element S_1/S_2. Three sets of results are compared, based on the CT-MQC algorithm (dark-green lines), FSSH (red lines), and corr-FSSH (cyan lines).

In order to assess the performance of the CT-MQC algorithm in capturing quantum decoherence,[71,72] we define an indicator of decoherence $\eta_{lk}(t) = N_{\text{tr}}^{-1}\sum_{I=1}^{N_{\text{tr}}}|C_l^{(I)*}(t)C_k^{(I)}(t)|^2$. The quantities $C_l^{(I)*}(t)C_k^{(I)}(t)$ stand for the off-diagonal elements of the electronic density matrix in the adiabatic representation and depend on nuclear positions through the dependence on the trajectory index I. $\eta_{lk}(t)$ can be evaluated on-the-fly during the dynamics, and besides being a valid measure of decoherence, it also provides complementary information to $\rho_l(t)$. Note that the same quantity is also used in the context of FSSH and corr-FSSH calculations, that is, $\eta_{lk}^{\text{FSSH}}(t)$ and $\eta_{lk}^{\text{corr-FSSH}}(t)$. Figure 1 (lower panel) shows that as the trajectories evolving on S_2 approach the S_1/S_2 conical intersection (between 5 and 10 fs) coherence between S_1 and S_2 builds up. We observe that, while after about 15 fs the nonadiabatic transition is complete, in FSSH, $\eta_{12}^{\text{FSSH}}(t)$ remains constant. This is the signature of the well-documented overcoherence problem in FSSH.[43,44,46,47,56−62] By contrast, $\eta_{12}^{\text{corr-FSSH}}(t)$ and $\eta_{12}(t)$ clearly show a decay, a consequence of the fact that the trajectories leave the nonadiabatic region (decoherence) and continue along different paths. As discussed in the introduction, the decoherence indicator proposed here will depend on the choice of representation used to describe the electronic states. Our particular choice has fallen on the Born−Oppenheimer (adiabatic) representation, which contains information simultaneously about electronic coherences and nuclear dynamics, via the parametric dependence of the adiabatic basis on the nuclear coordinates. This allows us to relate decoherence to the spatial separation in configuration space of different bundles of trajectories (and thus of different wavepackets), which "lose memory" of each other while

DOI: 10.1021/acs.jpclett.7b01249
J. Phys. Chem. Lett. 2017, 8, 3048−3055

evolving along diverging paths after funneling through the conical intersection. Henceforth, the analysis will be based on the comparison between CT-MQC and corr-FSSH as it is clear that only the FSSH algorithm with decoherence offers a valid benchmark to test our CT-MQC algorithm.

Figure 1 shows a pronounced double-peak structure in the $\eta_{12}(t)$ profile that is captured exclusively by the CT-MQC approach. This feature is an indication of the fact that two groups of trajectories funnel through the S_1/S_2 conical intersection at subsequent times. In order to capture this oscillation of the quantum coherence, the coupling of the trajectories taken into account in CT-MQC is essential; in fact, the corr-FSSH approach, which is based on the independent-trajectory approximation, misses this effect completely (see $\eta_{12}^{\text{corr-FSSH}}(t)$ in Figure 1). The wavepacket splitting at the S_1/S_2 conical intersection also coincides with the physical separation of the trajectories in configuration space. Figure 2 shows that

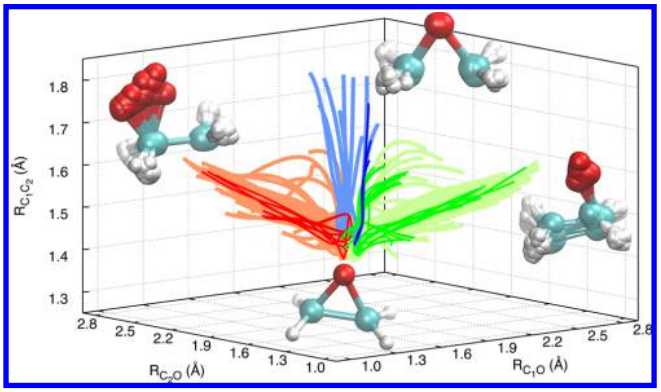

Figure 2. Identification of the three groups of trajectories that, starting from the initial geometries, yield right-open (red) or left-open (green) ring structures and CC-extended bond geometry (blue). The distributions of the final geometries are estimated as 36% (right-open structure), 47% (left-open structure), 10% (CC-extended bond structure), and 7% (closed-ring structure, not represented in the figure), based on CT-MQC dynamics, whereas they are 34% (right-open structure), 54% (left-open structure), 10% (CC-extended bond structure), and 2% (closed-ring structure, not represented in the figure), based on corr-FSSH dynamics. Light colors identify CT-MQC trajectories and darker colors corr-FSSH trajectories.

even though initialized with similar initial conditions, the trajectories yield different final structures. Analyzing the CT-MQC trajectories, we identified three major outcomes, (i) a right-open ring structure, (ii) a left-open ring structure, and (iii) a CC-extended bond structure. Figure 2 shows the trajectories plotted in the reduced space spanned by the three internal distances, namely, the C_1O, C_2O, and C_1C_2 bond lengths, which reproduce the splitting into the three groups (i)−(iii). The final structures corresponding to each trajectory are superimposed according to their grouping and depicted in Figure 2 using a ball−stick representation. Comparing CT-MQC with corr-FSSH trajectories, we observe that the latter display a more pronounced "classical" behavior as they appear to be more localized in space.

In Figure 3, we show the time evolution of the (normalized to the largest value) indicator of decoherence computed for the three different groups of trajectories, separately. In CT-MQC (upper panel), we observe that the first coherent peak arising between 6 and 12 fs is produced by a first bundle of trajectories that leads to breakage of the equivalent CO bonds. However,

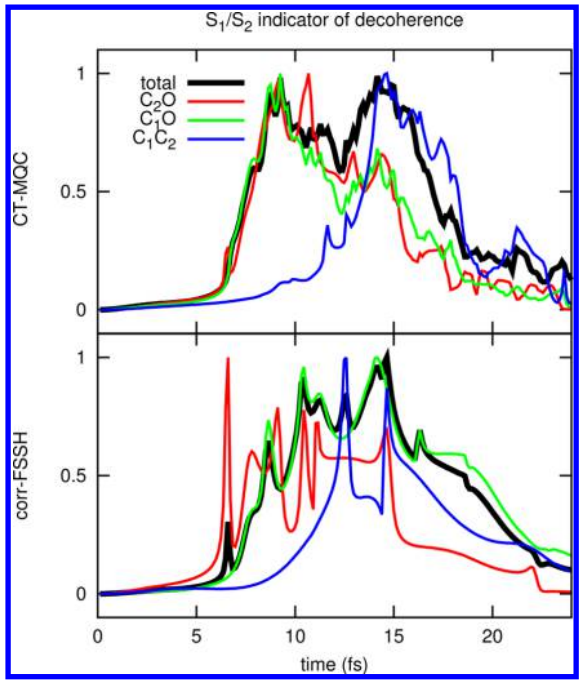

Figure 3. Normalized indicator of decoherence decomposed in three contributions arising from the different groups of trajectories identified in Figure 2. The labels C_1O and C_2O are used for the final left-open and right-open ring structures, respectively. The label C_1C_2 indicates the trajectories ending in a CC-extended bond configuration.

the decoherence indicator η_{12} associated with the C_1O and C_2O trajectory bundles does not decay in a monotonic fashion. Instead, both trajectory groups contribute to the formation of a second peak observed between 12 and 17.5 fs. The recoherence effect can be explained as follows: a first group of trajectories approaches at ∼6 fs the conical intersection, and during the crossing, they are reached by a second group at ∼12 fs. Due to the coupling among the trajectories, the first group, already on S_1, "feels" (through the quantum momentum) the approaching second group, and a revival of coherence is observed (second peak in the decoherence indicator of Figure 3). The main contribution to the second peak between 12 and 16 fs is given by trajectories yielding a final CC-extended bond structure. These trajectories clearly encounter the nonadiabatic region with some delay if compared to the sets of trajectories analyzed before (CO bond breaking). Here, the indicator of decoherence is clearly single-peaked, suggesting that the corresponding trajectory bundle undergoes a transition through the S_1/S_2 conical intersection in a single step. These trends are less evident when we analyze the corr-FSSH results in Figure 3 (lower panel). First, the double-peak nature of the decoherence indicator associated with the CO breaking bundles appears smeared out over the entire time interval (from ∼6 to 18 fs); this behavior is now associated with the uncorrelated recrossing of the nonadiabatic region by a subset of trajectories over an extended period of time (about 12 fs). Second, the contribution from the trajectory bundle associated with the CC bond breaking is simply associated with the delayed transition through the S_1/S_2 conical intersection. Overall, we also observe more noisy decoherence profiles in corr-FSSH. Again, this is a signature of the lack of coupling in the propagation of the corr-FSSH trajectories, which occurs within the independent trajectory approximation. This comparison also indicates that with the CT-MQC scheme satisfactory convergence can be

DOI: 10.1021/acs.jpclett.7b01249
J. Phys. Chem. Lett. 2017, 8, 3048−3055

achieved with about 100 trajectories, while more statistics is probably necessary for the corr-FSSH algorithm.

We now investigate the theoretical aspects associated with the achievements obtained with the CT-MQC scheme. The peculiar feature of the CT-MQC approach is the presence of the quantum momentum. Without the quantum momentum, the scheme reduces to a multitrajectory Ehrenfest approach and the coupling among the trajectories disappears. Being related to the spatial variation of the nuclear density, the quantum momentum embodies information about the "dispersion" of the trajectories in configuration space. In fact, it is possible to interpret the quantum momentum as the quantity that tracks the branching of the trajectories. Ehrenfest trajectories evolve according to a classical force determined from the average over the adiabatic potential energy surfaces, which hampers the possibility of spatial branching. The effect of the quantum momentum is to modify this average potential[70,92−96] by enabling groups of trajectories to evolve on purely adiabatic potential energy surfaces after separation in configuration space. This observation can be also verified by analyzing the time trace of the electronic populations along a single trajectory (Figure 4); when the populations are either 0 or 1 (1 being associated with the "force state", abuse of the surface-hopping language), only one adiabatic potential energy surface has nonzero contribution in the expression of the classical force; when the trajectory crosses the conical intersection, the populations have values between 0 and 1 because of the amplitude exchange driven by the nonadiabatic coupling vectors. After leaving the nonadiabatic region, the coupling among the trajectories becomes essential, and if groups of trajectories separate in space, decoherence builds in with the effect of "collapsing" the electronic populations to either 0 or 1. It becomes therefore evident that the quantum momentum has the same overall effect on the electronic populations as the decoherence corrections on the surface-hopping algorithm adopted here. However, differently from corr-FSSH, the quantum momentum is derived from the exact evolution equations and is not of phenomenological nature. Figure 4 (upper panel) clearly exemplifies this effect by showing the time evolution of the S_1 and S_2 states' populations calculated along a representative trajectory. For this particular trajectory, FSSH predicts that the electronic populations of S_1 and S_2 after crossing the nonadiabatic region remain between 0 and 1. Decoherence corrections, however, enforce the collapse of the populations (S_1 to 1 and S_2 to 0) as in the case of corr-FSSH. Exactly the same behavior is observed with CT-MQC, with the difference that the decoherence is *derived* from an exact solution. Figure 4 (lower panel) also shows the time-dependent potential energy surface (TDPES), $\epsilon_{\mathrm{GI}}^{(I)}(t) = \sum_k |C_l^{(I)}(t)|^2 \epsilon_{\mathrm{BO}}^{(k),(I)}$, for a representative trajectory, compared to the energy of the force state in corr-FSSH. Both surfaces show similar profiles; in fact, in corr-FSSH, the force state switches abruptly from S_2 to S_1 at the conical intersection (high swap probability), whereas in CT-MQC, $\epsilon_{\mathrm{GI}}^{(I)}(t)$ describes a diabatic surface that smoothly evolves from S_2 to S_1 at the conical intersection.

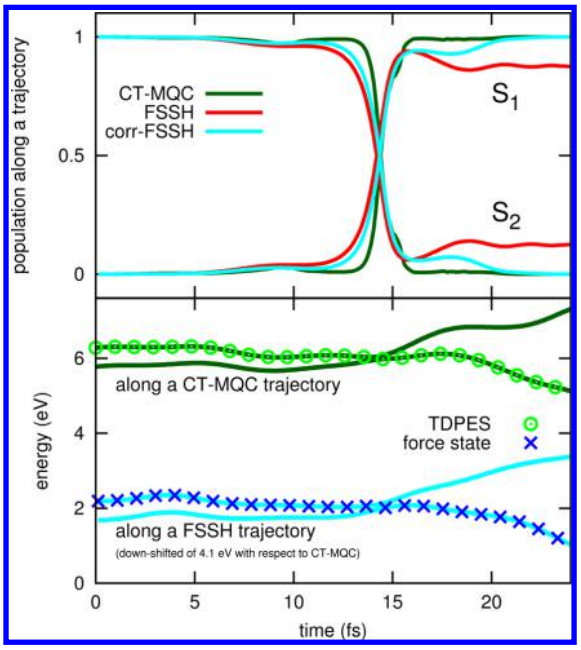

Figure 4. Upper panel: Time trace of the electronic populations of S_1 and S_2 for a selected trajectory. Three sets of results are shown, CT-MQC (dark-green lines), FSSH (red lines), and corr-FSSH (cyan lines). Lower panel: Adiabatic potential energy surfaces for S_1 and S_2 along the selected trajectory generated by CT-MQC (dark-green lines) and by corr-FSSH (cyan lines). The zero of the energy scale is set to the value of the ground-state potential energy at the initial time. The surfaces corresponding to corr-FSSH are downshifted by 4.1 eV in comparison to CT-MQC. TDPES (green circles) stands for the gauge-invariant part of the scalar potential, that is, $\langle \Phi_R(t)|\hat{H}_{\mathrm{BO}}|\Phi_R(t)\rangle_r$ estimated here as $\epsilon_{\mathrm{GI}}^{(I)}(t) = \sum_k |C_k^{(I)}(t)|^2 \epsilon_{\mathrm{BO}}^{(k),(I)}$; force state (blue crosses) stands for the energy of the populated electronic state along the corr-FSSH trajectory used for computing the classical force.

Computationally, the cost of CT-MQC calculations is slightly larger than that in the case of FSSH. This is mainly due to the fact that in CT-MQC nuclear forces receive contributions from all electronic states and therefore a force calculation for each state included in the dynamics is required at each step. In addition, the presence of couplings among the trajectories (through the quantum momentum) makes the parallelization of the electronic structure calculation and the distribution of the trajectories over different cores important requirements for an efficient implementation of this MQC scheme.

In summary, we have reported the first application of the CT-MQC algorithm derived from exact factorization to the study of the photochemistry of a molecule in the gas phase, namely, the photoinduced ring-opening in oxirane. The approach correctly captures quantum decoherence without the need for empirical corrections to damp state populations away from the regions of strong nonadiabatic couplings. The quality of the CT-MQC results was assessed by comparing with FSSH, without and with phenomenological decoherence corrections. The CT-MQC approach derived from the exact factorization yields a coupled-trajectory nonadiabatic dynamics with built-in decoherence, providing, therefore, a rigorous solution to the overcoherence issue in standard FSSH. In addition, the coupling among the trajectories induced by the quantum momentum improves the *quantumness* of the trajectory bundle that behaves now as a quantum wavepacket, solving many drawbacks of conventional FSSH and improving the convergence of the calculations with the number of trajectories.

All calculations were performed with CPMD[84] employing the PBE[91] functional for ground-state and excited-state calculations. Linear-response TDDFT calculations were based on the Tamm−Dancoff approximation.[97,98] The Kleinman−Bylander[99] pseudopotential was used for all atom species together

DOI: 10.1021/acs.jpclett.7b01249
J. Phys. Chem. Lett. 2017, 8, 3048−3055

with a plane-wave cutoff of 70 Ry. Initial conditions, that is, positions and momenta, were sampled from an ab initio ground-state 2 ps trajectory at 300 K. N_{tr} = 100 trajectories are propagated with a time step of 0.12 fs (5 au) for both CT-MQC and (corr-)FSSH dynamics. For the surface-hopping calculations, only 20 initial conditions were selected from the ground-state thermalization, each giving rise to 5 trajectories with different jump histories. The parameters used in corr-FSSH are reported in ref 44.

■ ASSOCIATED CONTENT

Supporting Information

The Supporting Information is available free of charge on the ACS Publications website at DOI: 10.1021/acs.jpclett.7b01249.

Comprehensive details on the CT-MQC algorithm and on linear-response TDDFT (PDF)

■ AUTHOR INFORMATION

Corresponding Authors

*E-mail: skmin@unist.ac.kr (S.K.M.).
*E-mail: federica.agostini@u-psud.fr (F.A.).

ORCID

Seung Kyu Min: 0000-0001-5636-3407
Federica Agostini: 0000-0003-2951-4964
Ivano Tavernelli: 0000-0001-5690-1981

Notes

The authors declare no competing financial interest.

■ ACKNOWLEDGMENTS

S.K.M. acknowledges financial support from the Basic Science Research Program through the National Research Foundation of Korea (NRF) funded by the Ministry of Education (2016R1C1B2015103) and the 2015 Research Fund (1.150115.01) of UNIST (Ulsan National Institute of Science & Technology). I.T. acknowledges the Swiss National Centres of Competence in Research (NCCR) MARVEL for its support.

■ REFERENCES

(1) Engel, G. S.; Calhoun, T. R.; Read, E. L.; Ahn, T.-K.; Mančal, T.; Cheng, Y.-C.; Blankenship, R. E.; Fleming, G. R. Evidence for Wavelike Energy Transfer through Quantum Coherence in Photosynthetic Systems. *Nature* **2007**, *446*, 782−786.

(2) Ishizaki, A.; Fleming, G. R. Theoretical Examination of Quantum Coherence in a Photosynthetic System at Physiological Temperature. *Proc. Natl. Acad. Sci. U. S. A.* **2009**, *106*, 17255−17260.

(3) Scholes, G. D. Quantum Coherent Electronic Energy Transfer: Did Nature Think of It First? *J. Phys. Chem. Lett.* **2010**, *1*, 2−8.

(4) Collini, E.; Wong, C. Y.; Wilk, K. E.; Curmi, P. M. G.; Brumer, P.; Scholes, G. D. Coherently Wired Light-Harvesting in Photosynthetic Marine Algae at Ambient Temperature. *Nature* **2010**, *463*, 644−647.

(5) Panitchayangkoon, G.; Hayes, D.; Fransted, K. A.; Caram, J. R.; Harel, E.; Wen, J.; Blankenship, R. E.; Engel, G. S. Long-Lived Quantum Coherence in Photosynthetic Complexes at Physiological Temperature. *Proc. Natl. Acad. Sci. U. S. A.* **2010**, *107*, 12766−12770.

(6) Turner, D. B.; Wilk, K. E.; Curmi, P. M. G.; Scholes, G. D. Comparison of Electronic and Vibrational Coherence Measured by Two-Dimensional Electronic Spectroscopy. *J. Phys. Chem. Lett.* **2011**, *2*, 1904−1911.

(7) Huo, P.; Coker, D. F. Theoretical Study of Coherent Excitation Energy Transfer in Cryptophyte Phycocyanin 645 at Physiological Temperature. *J. Phys. Chem. Lett.* **2011**, *2*, 825−833.

(8) Strümpfer, J.; Sener, M.; Schulten, K. How Quantum Coherence Assists Photosynthetic Light-Harvesting. *J. Phys. Chem. Lett.* **2012**, *3*, 536−542.

(9) Dorfman, K. E.; Voronine, D. V.; Mukamel, S.; Scully, M. O. Photosynthetic Reaction Center as a Quantum Heat Engine. *Proc. Natl. Acad. Sci. U. S. A.* **2013**, *110*, 2746−2751.

(10) Rozzi, C. A.; Falke, S. M.; Spallanzani, N.; Rubio, A.; Molinari, E.; Brida, D.; Maiuri, M.; Cerullo, G.; Schramm, H.; Christoffers, J.; et al. Quantum Coherence Controls the Charge Separation in a Prototypical Artificial Light-Harvesting System. *Nat. Commun.* **2013**, *4*, 1602.

(11) Akimov, A. V.; Prezhdo, O. V. Persistent Electronic Coherence Despite Rapid Loss of Electron-Nuclear Correlation. *J. Phys. Chem. Lett.* **2013**, *4*, 3857−3864.

(12) Landry, B. R.; Subotnik, J. E. Quantifying the Lifetime of Triplet Energy Transfer Processes in Organic Chromophores: A Case Study of 4-(2-Naphthylmethyl)benzaldehyde. *J. Chem. Theory Comput.* **2014**, *10*, 4253−4263.

(13) Curutchet, C.; Mennucci, B. Quantum Chemical Studies of Light Harvesting. *Chem. Rev.* **2017**, *117*, 294−343.

(14) Meyer, H.-D.; Manthe, U.; Cederbaum, L. S. The Multi-Configurational Time-Dependent Hartree Approach. *Chem. Phys. Lett.* **1990**, *165*, 73−78.

(15) Burghardt, I.; Meyer, H.-D.; Cederbaum, L. S. Approaches to the Approximate Treatment of Complex Molecular Systems by the Multiconfiguration Time-Dependent Hartree Method. *J. Chem. Phys.* **1999**, *111*, 2927−2939.

(16) Meyer, H.-D.; Worth, G. A. Quantum Molecular Dynamics: Propagating Wavepackets and Density Operators Using the Multi-configuration Time-Dependent Hartree Method. *Theor. Chim. Acta* **2003**, *109*, 251−267.

(17) Thoss, M.; Domcke, W.; Wang, H. Theoretical Study of Vibrational Wave-Packet Dynamics in Electron-Transfer Systems. *Chem. Phys.* **2004**, *296*, 217−229.

(18) Li, J.; Kondov, I.; Wang, H.; Thoss, M. Theoretical Study of Photoinduced Electron-Transfer Processes in the Dye-Semiconductor System Alizarin-TiO_2. *J. Phys. Chem. C* **2010**, *114*, 18481−18493.

(19) Meng, Q.; Faraji, S.; Vendrell, O.; Meyer, H.-D. Full Dimensional Quantum-Mechanical Simulations for the Vibronic Dynamics of Difluorobenzene Radical Cation Isomers Using the Multilayer Multiconfiguration Time-Dependent Hartree Method. *J. Chem. Phys.* **2012**, *137*, 134302.

(20) Martínez, T. J.; Levine, R. D. Dynamics of the Collisional Electron Transfer and Femtosecond Photodissociation of NaI on Ab Initio Electronic Energy Curves. *Chem. Phys. Lett.* **1996**, *259*, 252−260.

(21) Martínez, T. J.; Ben-Nun, M.; Levine, R. D. Multi-Electronic-State Molecular Dynamics: A Wave Function Approach. *J. Phys. Chem.* **1996**, *100*, 7884−7895.

(22) Martìnez, T. J. Insights for Light-Driven Molecular Devices from Ab Initio Multiple Spawning Excited-State Dynamics of Organic and Biological Chromophores. *Acc. Chem. Res.* **2006**, *39*, 119−126.

(23) Briggs, J. S.; Eisfeld, A. Equivalence of Quantum and Classical Coherence in Electronic Energy Transfer. *Phys. Rev. E* **2011**, *83*, 051911.

(24) Miller, W. H. Quantum or Classical Coherence? *J. Chem. Phys.* **2012**, *136*, 210901.

(25) O'Reilly, E. J.; Olaya-Castro, A. Non-Classicality of the Molecular Vibrations Assisting Exciton Energy Transfer at Room Temperature. *Nat. Commun.* **2014**, *5*, 3012.

(26) Arpin, P. C.; Turner, D. B.; McClure, S. D.; Jumper, C. C.; Mirkovic, T.; Challa, J. R.; Lee, J.; Teng, C. Y.; Green, B. R.; Wilk, K. E.; et al. Spectroscopic Studies of Cryptophyte Light Harvesting Proteins: Vibrations and Coherent Oscillations. *J. Phys. Chem. B* **2015**, *119*, 10025−10034.

(27) Kapral, R.; Ciccotti, G. Mixed Quantum-Classical Dynamics. *J. Chem. Phys.* **1999**, *110*, 8919−8929.

(28) Nielsen, S.; Kapral, R.; Ciccotti, G. Mixed Quantum-Classical Surface Hopping Dynamics. *J. Chem. Phys.* **2000**, *112*, 6543−6553.

(29) Kapral, R. Progress in the Theory of Mixed Quantum-Classical Dynamics. *Annu. Rev. Phys. Chem.* **2006**, *57*, 129−157.

DOI: 10.1021/acs.jpclett.7b01249
J. Phys. Chem. Lett. 2017, 8, 3048−3055

(30) Grunwald, R.; Kim, H.; Kapral, R. Surface-Hopping Dynamics and Decoherence with Quantum Equilibrium Structure. *J. Chem. Phys.* **2008**, *128*, 164110.
(31) Jang, S. Nonadiabatic Quantum Liouville and Master Equations in the Adiabatic Basis. *J. Chem. Phys.* **2012**, *137*, 22A536.
(32) Kelly, A.; Markland, T. E. Efficient and Accurate Surface Hopping for Long Time Nonadiabatic Quantum Dynamics. *J. Chem. Phys.* **2013**, *139*, 014104.
(33) Bonella, S.; Coker, D. F. LAND-map, a Linearized Approach to Nonadiabatic Dynamics using the Mapping Formalism. *J. Chem. Phys.* **2005**, *122*, 194102.
(34) Dunkel, E. R.; Bonella, S.; Coker, D. F. Iterative Linearized Approach to Nonadiabatic Dynamics. *J. Chem. Phys.* **2008**, *129*, 114106.
(35) Huo, P.; Coker, D. F. Consistent Schemes for Non-Adiabatic Dynamics Derived from Partial Linearized Density Matrix Propagation. *J. Chem. Phys.* **2012**, *137*, 22A535.
(36) Curchod, B. F. E.; Tavernelli, I.; Rothlisberger, U. Trajectory-Based Solution of the Nonadiabatic Quantum Dynamics Equations: an On-the-Fly Approach for Molecular Dynamics Simulations. *Phys. Chem. Chem. Phys.* **2011**, *13*, 3231−3236.
(37) Curchod, B. F. E.; Tavernelli, I. On Trajectory-Based Nonadiabatic Dynamics: Bohmian Dynamics Versus Trajectory Surface Hopping. *J. Chem. Phys.* **2013**, *138*, 184112.
(38) Albareda, G.; Bofill, J. M.; Tavernelli, I.; Huarte-Larrañaga, F.; Illas, F.; Rubio, A. Conditional Born-Oppenheimer Dynamics: Quantum Dynamics Simulations for the Model Porphine. *J. Phys. Chem. Lett.* **2015**, *6*, 1529−1535.
(39) Prezhdo, O. V. Mean Field Approximation for the Stochastic Schrödinger Equation. *J. Chem. Phys.* **1999**, *111*, 8366−8377.
(40) Bedard-Hearn, M. J.; Larsen, R. E.; Schwartz, B. J. Mean-Field Dynamics with Stochastic Decoherence (MF-SD): A New Algorithm for Nonadiabatic Mixed Quantum/Classical Molecular-Dynamics Simulations with Nuclear-Induced Decoherence. *J. Chem. Phys.* **2005**, *123*, 234106.
(41) Alonso, J. L.; Clemente-Gallardo, J.; Cuchí, J. C.; Echenique, P.; Falceto, F. Ehrenfest Dynamics is Purity Non-Preserving: A Necessary Ingredient for Decoherence. *J. Chem. Phys.* **2012**, *137*, 054106.
(42) Akimov, A. V.; Long, R.; Prezhdo, O. V. Coherence Penalty Functional: A Simple Method for Adding Decoherence in Ehrenfest Dynamics. *J. Chem. Phys.* **2014**, *140*, 194107.
(43) Jasper, A. W.; Nangia, S.; Zhu, C.; Truhlar, D. G. Non-Born-Oppenheimer Molecular Dynamics. *Acc. Chem. Res.* **2006**, *39*, 101−108.
(44) Granucci, G.; Persico, M. Critical Appraisal of the Fewest Switches Algorithm for Surface Hopping. *J. Chem. Phys.* **2007**, *126*, 134114.
(45) Jaeger, H. M.; Fischer, S.; Prezhdo, O. V. Decoherence-Induced Surface Hopping. *J. Chem. Phys.* **2012**, *137*, 22A545.
(46) Subotnik, J. E.; Ouyang, W.; Landry, B. R. Can We Derive Tully's Surface-Hopping Algorithm from the Semiclassical Quantum Liouville Equation? Almost, but only with Decoherence. *J. Chem. Phys.* **2013**, *139*, 214107.
(47) Gao, X.; Thiel, W. Non-Hermitian Surface Hopping. *Phys. Rev. E: Stat. Phys., Plasmas, Fluids, Relat. Interdiscip. Top.* **2017**, *95*, 013308.
(48) Wang, L.; Akimov, A.; Prezhdo, O. V. Recent Progress in Surface Hopping: 2011−2015. *J. Phys. Chem. Lett.* **2016**, *7*, 2100−2112.
(49) Craig, C. F.; Duncan, W. R.; Prezhdo, O. V. Trajectory Surface Hopping in the Time-Dependent Kohn-Sham Approach for Electron-Nuclear Dynamics. *Phys. Rev. Lett.* **2005**, *95*, 163001.
(50) Tapavicza, E.; Tavernelli, I.; Rothlisberger, U. Trajectory Surface Hopping within Linear Response Time-Dependent Density-Functional Theory. *Phys. Rev. Lett.* **2007**, *98*, 023001.
(51) Doltsinis, N. L.; Marx, D. Nonadiabatic Car-Parrinello Molecular Dynamics. *Phys. Rev. Lett.* **2002**, *88*, 166402.
(52) Jasper, A. W.; Zhu, C.; Nangia, S.; Truhlar, D. G. Introductory Lecture: Nonadiabatic Effects in Chemical Dynamics. *Faraday Discuss.* **2004**, *127*, 1−22.
(53) Tully, J. C.; Preston, R. Trajectory Surface Hopping Approach to Nonadiabatic Molecular Collisions: The Reaction of H^+ with D_2. *J. Chem. Phys.* **1971**, *55*, 562−572.
(54) Tully, J. C. Molecular Dynamics with Electronic Transitions. *J. Chem. Phys.* **1990**, *93*, 1061−1071.
(55) Penfold, T. J.; Worth, G. A. The Photodissociation of Ozone: A Quasi-Classical Approach to a Quantum Dynamics Problem. *J. Mol. Graphics Modell.* **2007**, *26*, 613−621.
(56) Schwartz, B. J.; Bittner, E. R.; Prezhdo, O. V.; Rossky, P. J. Quantum Decoherence and the Isotope Effect in Condensed Phase Nonadiabatic Molecular Dynamics Simulations. *J. Chem. Phys.* **1996**, *104*, 5942−5955.
(57) Fang, J.-Y.; Hammes-Schiffer, S. Improvement of the Internal Consistency in Trajectory Surface Hopping. *J. Phys. Chem. A* **1999**, *103*, 9399−9407.
(58) Shenvi, N.; Subotnik, J. E.; Yang, W. Simultaneous-Trajectory Surface Hopping: A Parameter-Free Algorithm for Implementing Decoherence in Nonadiabatic Dynamics. *J. Chem. Phys.* **2011**, *134*, 144102.
(59) Shenvi, N.; Subotnik, J. E.; Yang, W. Phase-corrected surface hopping: Correcting the Phase Evolution of the Electronic Wavefunction. *J. Chem. Phys.* **2011**, *135*, 024101.
(60) Shenvi, N.; Yang, W. Achieving Partial Decoherence in Surface Hopping through Phase Correction. *J. Chem. Phys.* **2012**, *137*, 22A528.
(61) Subotnik, J. E.; Shenvi, N. A New Approach to Decoherence and Momentum Rescaling in the Surface Hopping Algorithm. *J. Chem. Phys.* **2011**, *134*, 024105.
(62) Subotnik, J. E.; Shenvi, N. Decoherence and Surface Hopping: When Can Averaging over Initial Conditions Help Capture the Effects of Wave Packet Separation? *J. Chem. Phys.* **2011**, *134*, 244114.
(63) Abedi, A.; Maitra, N. T.; Gross, E. K. U. Exact Factorization of the Time-Dependent Electron-Nuclear Wave Function. *Phys. Rev. Lett.* **2010**, *105*, 123002.
(64) Abedi, A.; Maitra, N. T.; Gross, E. K. U. Correlated Electron-Nuclear Dynamics: Exact Factorization of the Molecular Wavefunction. *J. Chem. Phys.* **2012**, *137*, 22A530.
(65) Abedi, A.; Agostini, F.; Gross, E. K. U. Mixed Quantum-Classical Dynamics from the Exact Decomposition of Electron-Nuclear Motion. *Europhys. Lett.* **2014**, *106*, 33001.
(66) Agostini, F.; Abedi, A.; Gross, E. K. U. Classical Nuclear Motion Coupled to Electronic Non-Adiabatic Transitions. *J. Chem. Phys.* **2014**, *141*, 214101.
(67) Agostini, F.; Min, S. K.; Gross, E. K. U. Semiclassical Analysis of the Electron-Nuclear Coupling in Electronic Non-Adiabatic Processes. *Ann. Phys.* **2015**, *527*, 546−555.
(68) Suzuki, Y.; Abedi, A.; Maitra, N. T.; Gross, E. K. U. Laser-Induced Electron Localization in H_2^+: Mixed Quantum-Classical Dynamics Based on the Exact Time-Dependent Potential Energy Surface. *Phys. Chem. Chem. Phys.* **2015**, *17*, 29271−29280.
(69) Suzuki, Y.; Abedi, A.; Maitra, N. T.; Yamashita, K.; Gross, E. K. U. Electronic Schrödinger Equation with Nonclassical Nuclei. *Phys. Rev. A: At., Mol., Opt. Phys.* **2014**, *89*, 040501.
(70) Agostini, F.; Abedi, A.; Suzuki, Y.; Min, S. K.; Maitra, N. T.; Gross, E. K. U. The Exact Forces on Classical Nuclei in Non-Adiabatic Charge Transfer. *J. Chem. Phys.* **2015**, *142*, 084303.
(71) Min, S. K.; Agostini, F.; Gross, E. K. U. Coupled-Trajectory Quantum-Classical Approach to Electronic Decoherence in Non-adiabatic Processes. *Phys. Rev. Lett.* **2015**, *115*, 073001.
(72) Agostini, F.; Min, S. K.; Abedi, A.; Gross, E. K. U. Quantum-Classical Non-Adiabatic Dynamics: Coupled- vs. Independent-Trajectory Methods. *J. Chem. Theory Comput.* **2016**, *12*, 2127−2143.
(73) Dou, W.; Subotnik, J. E. A Many-Body States Picture of Electronic Friction: The Case of Multiple Orbitals and Multiple Electronic States. *J. Chem. Phys.* **2016**, *145*, 054102.
(74) Schneider, E.; a Beccara, S.; Mascherpa, F.; Faccioli, P. Quantum Propagation of Electronic Excitations in Macromolecules: A Computationally Efficient Mutliscale Approach. *Phys. Rev. B: Condens. Matter Mater. Phys.* **2016**, *94*, 0143061.

DOI: 10.1021/acs.jpclett.7b01249
J. Phys. Chem. Lett. 2017, 8, 3048−3055

(75) White, A.; Tretiak, S.; Mozyrsky, D. Coupled Wave-Packets for Non-Adiabatic Molecular Dynamics: a Generaliztion of Gaussian Wave-Packet Dynamics to Multiple Potential Energy Surfaces. *Chem. Sci.* **2016**, *7*, 4905−4911.
(76) Runge, E.; Gross, E. K. U. Density-Functional Theory for Time-Dependent Systems. *Phys. Rev. Lett.* **1984**, *52*, 997−1000.
(77) Casida, M. E. In *Recent Advances in Density Functional Methods*; Chong, D. P., Ed.; World Scientific: Singapore, 1995; p 155.
(78) Grabo, T.; Petersilka, M.; Gross, E. K. U. Molecular Excitation Energies from Time- Dependent Density Functional Theory. *J. Mol. Struct.: THEOCHEM* **2000**, *501−502*, 353.
(79) de Carvalho, F. F.; Bouduban, M. E. F.; Curchod, B. F. E.; Tavernelli, I. Nonadiabatic Molecular Dynamics Based on Trajectories. *Entropy* **2014**, *16*, 62−85.
(80) Eich, F. G.; Agostini, F. The Adiabatic Limit of the Exact Factorization of the Electron-Nuclear Wave Function. *J. Chem. Phys.* **2016**, *145*, 054110.
(81) Scherrer, A.; Agostini, F.; Sebastiani, D.; Gross, E. K. U.; Vuilleumier, R. Nuclear Velocity Perturbation Theory for Vibrational Circular Dichroism: An Approach Based on the Exact Factorization of the Electron-Nuclear Wave Function. *J. Chem. Phys.* **2015**, *143*, 074106.
(82) Scherrer, A.; Agostini, F.; Sebastiani, D.; Gross, E. K. U.; Vuilleumier, R. On the Mass of Atoms in Molecules: Beyond the Born-Oppenheimer Approximation. arXiv:1605.04211 [physics.chem-ph] **2016**.
(83) Garashchuk, S.; Rassolov, V. A. Quantum Dynamics with Bohmian Trajectories: Energy Conserving Approximation to the Quantum Potential. *Chem. Phys. Lett.* **2003**, *376*, 358−363.
(84) CPMD. http://www.cpmd.org/, Copyright IBM Corp 1990−2015, Copyright MPI für Festkörperforschung Stuttgart (1997−2001).
(85) Tavernelli, I.; Curchod, B. F. E.; Laktionov, A.; Rothlisberger, U. Nonadiabatic Coupling Vectors for Excited States within Time-Dependent Density Functional Theory in the Tamm-Dancoff Approximation and Beyond. *J. Chem. Phys.* **2010**, *133*, 194104.
(86) Hu, C.; Sugino, O.; Watanabe, K. Second-Order Nonadiabatic Couplings from Time-Dependent Density Functional Theory: Evaluation in the Immediate Vicinity of Jahn-Teller/Renner-Teller Intersections. *J. Chem. Phys.* **2011**, *135*, 074101.
(87) Haruyama, J.; Suzuki, T.; Hu, C.; Watanabe, K. Excited-State Nuclear Forces on Adiabatic Potential-Energy Surfaces by Time-Dependent Density-Functional Theory. *Phys. Rev. A: At., Mol., Opt. Phys.* **2012**, *85*, 012516.
(88) Curchod, B. F. E.; Rothlisberger, U.; Tavernelli, I. Trajectory-Based Nonadiabatic Dynamics with Time-Dependent Density Functional Theory. *ChemPhysChem* **2013**, *14*, 1314−1340.
(89) Cordova, F.; Doriol, L. J.; Ipatov, A.; Casida, M. E.; Filippi, C.; Vela, A. Troubleshooting Time-Dependent Density-Functional Theory for Photochemical Applications: Oxirane. *J. Chem. Phys.* **2007**, *127*, 164111.
(90) Tapavicza, E.; Tavernelli, I.; Rothlisberger, U.; Filippi, C.; Casida, M. E. Mixed Time-Dependent Density-Functional Theory/Classical Trajectory Surface Hopping Study of Oxirane Photochemistry. *J. Chem. Phys.* **2008**, *129*, 124108.
(91) Perdew, J. P.; Burke, K.; Ernzerhof, M. Generalized Gradient Approximation Made Simple. *Phys. Rev. Lett.* **1996**, *77*, 3865−3868.
(92) Abedi, A.; Agostini, F.; Suzuki, Y.; Gross, E. K. U. Dynamical Steps That Bridge Piecewise Adiabatic Hhapes in the Exact Time-Dependent Potential Energy Surface. *Phys. Rev. Lett.* **2013**, *110*, 263001.
(93) Agostini, F.; Abedi, A.; Suzuki, Y.; Gross, E. K. U. Mixed Quantum-Classical Dynamics on the Exact Time-Dependent Potential Energy Surfaces: A Novel Perspective on Non-Adiabatic Processes. *Mol. Phys.* **2013**, *111*, 3625−3640.
(94) Curchod, B. F. E.; Agostini, F.; Gross, E. K. U. An exact factorization perspective on quantum interferences in nonadiabatic dynamics. *J. Chem. Phys.* **2016**, *145*, 034103.
(95) Curchod, B. F. E.; Agostini, F. On the Dynamics through a Conical Intersection. *J. Phys. Chem. Lett.* **2017**, *8*, 831−837.
(96) Khosravi, E.; Abedi, A.; Maitra, N. T. Exact Potential Driving the Electron Dynamics in Enhanced Ionization of H_2^+. *Phys. Rev. Lett.* **2015**, *115*, 263002.
(97) Tamm, I. *J. Phys. (USSR)* **1945**, *9*, 449.
(98) Dancoff, S. M. Non-Adiabatic Meson Theory of Nuclear Forces. *Phys. Rev.* **1950**, *78*, 382−385.
(99) Kleinman, L.; Bylander, D. M. Efficacious Form for Model Pseudopotentials. *Phys. Rev. Lett.* **1982**, *48*, 1425−1428.

DOI: 10.1021/acs.jpclett.7b01249
J. Phys. Chem. Lett. 2017, 8, 3048−3055